Current Research in MRI

Original Article

The Role of Multiparametric Scrotal Magnetic Resonance Imaging in the Histological Differentiation of Germ Cell Neoplasia In Situ-Related Testicular Germ Cell Tumors: Can Seminomatous and Mixed-Non-Seminomatous Germ Cell Tumors Be Separated?

Serdar Aslan[1], Uluhan Eryürük[1], Ural Oğuz[2], İsmet Miraç Çakır[1,3]

[1]Department of Radiology, Giresun University Faculty of Medicine, Giresun, Turkey
[2]Department of Urology, Giresun University Faculty of Medicine, Giresun, Turkey
[3]Department of Radiology, Samsun Education and Research Hospital, Samsun, Turkey

Cite this article as: Aslan S, Eryürük U, Oğuz U, Çakır İM. The role of multiparametric scrotal Magnetic Resonance Imaging in the histological differentiation of germ cell neoplasia insitu-related testicular germ cell tumors: Can seminomatous and mixed-non-seminomatous germ cell tumors be separated? *Current Research in MRI* 2023;2(3):63-69.

Corresponding author: Uluhan Eryürük, e-mail: uluhaneryuruk@gmail.com

Received: September 27, 2023 **Accepted:** October 15, 2023 **Publication Date:** October 30, 2023

DOI:10.5152/CurrResMRI.2023.23078

Abstract

Objective: The aim was to examine the efficacy of multiparametric magnetic resonance imaging (mp-MRI) in the histological differentiation of germ cell neoplasia in situ (GCNIS)-related testicular germ cell tumors (TGCTs).

Methods: We retrospectively included 58 patients with histologically proven GCNIS-related TGCTs, who underwent mp-MRI between November 2019 and June 2022. The signal characteristics of the tumors on T2-weighted imaging were recorded. The mean apparent diffusion coefficient (ADC) values were calculated. Time signal intensity curves were generated, and semiquantitative parameters were calculated. The presence of a septal enhancement pattern within the tumor was noted. Receiver operating characteristic curve analysis was performed to assess the diagnostic performance of the parameters.

Results: Histopathological examination revealed that 24 of the cases were seminomas, and 10 were non-seminomatous GCT (NSGCTs). The incidence of hypointense signals was notably higher for seminomas ($P < .001$). The mean ADC values of the seminomas were lower than NSGCTs (0.645 ± 0.11 and 0.879 ± 0.061, respectively, $P < .001$). The optimal ADC cutoff value was 0.779×10^{-3} mm^2/s. No differences were observed between the 2 groups for semiquantitative parameters ($P = .16$-$.83$). However, the septal enhancement pattern was more frequent in seminomas ($P = .002$).

Conclusion: Values of ADC measured in mp-MRI can be used as a reliable preoperative method in the histological differentiation of GCNIS-related TGCTs. Also, the septal enhancement pattern can be helpful in distinguishing between seminoma and NSGCT.

Keywords: Germ cell neoplasia in situ-related testicular germ cell tumors, magnetic resonance imaging, apparent diffusion coefficient, dynamic contrast-enhanced imaging, differential diagnosis

INTRODUCTION

Testicular cancer (TC) represents approximately 1% of male neoplasms.[1] However, it represents the most common type of cancer in the male demographic aged 15-35 years, contributing to approximately 10%-14% of cancer cases in this age group.[1,2] It is estimated by the American Cancer Society that in 2022, 9910 men will develop TC, and 460 men will die from this disease.[3] Most TCs are testicular germ cell tumors (TGCTs) originating from the germinal epithelium of the seminiferous tubules.[4,5] The TGCTs are divided into 2 groups: germ cell neoplasia in situ (GCNIS)-related TGCTs and non-GCNIS-related TGCTs. The GCNIS-related TGCTs are also divided into 3 groups: seminomas, mixed-non-seminomatous GCT (NSGCT), and burned-out GCTs. Seminomas and mixed-NSGCT constitute the majority of GCNIS-related TGCTs.[6] The general morphology and histological features of these 2 broad tumor groups differ from each other, and it is emphasized that this situation is related to imaging features.[7-10]

Radical orchiectomy is the preferred therapeutic approach for cases of TGCTs associated with GCNIS and should be carried out promptly unless clinical circumstances necessitate immediate chemotherapy.[11] In these cases, a noninvasive imaging modality would be of great benefit to help predict the histological characteristics of GCNIS-related TGCTs preoperatively.

Currently, ultrasonography (US) is accepted as the first choice for the diagnostic imaging of testicular masses.[12-14] However, changes in echogenicity may not be specific, and reliable characterization of testicular masses is not always possible.[15-19]

Recently, it has been shown that magnetic resonance imaging (MRI) shows high diagnostic performance for both morphological evaluation and tissue characterization in testicular masses.[8-10,15,17-19] The benefits of this technique encompass concurrent multi-plane imaging of both testes and paratesticular areas, providing high contrast and spatial resolution, offering satisfactory anatomical and functional information, with no radiation exposure, and exhibiting reduced reliance on the operator when contrasted with US.[14,18,20] Previous studies showed that conventional MRI features of GCNIS-related TGCTs are closely related to histological features and that diffusion-weighted images (DWIs) and dynamic contrast-enhanced (DCE) images play an important role in the characterization of scrotal masses.[7-9,17-19,21,22] However, all of these studies separately compared the MRI features of GCNIS-related TGCTs with histological features.

To the best of our knowledge, there is no study that correlates multiparametric magnetic resonance imaging (mp-MRI) findings with histological features. Our aim in this study is to investigate the efficacy of mp-MRI in distinguishing between seminoma and mixed-NSGCT.

METHODS

Approval for this retrospective study was granted by the Institutional Ethics Committee (Ethics Committee number: KAEK-108, date: March 18, 2021, Giresun University). Given its retrospective nature, necessity for informed consent was waived.

Study Population

A search of our institutional electronic medical database was performed to identify patients who met the specified inclusion criteria for the period spanning from November 2019 to June 2022: patients who (1) had histopathological evidence of GCNIS-related TGCTs after radical orchiectomy and (2) underwent an mp-MRI scan. The exclusion criteria included (1) unsatisfactory image quality and (2) mainly hemorrhagic and/or necrotic tumors. In the case of bilateral tumors, each tumor was evaluated separately. The final study population comprised 30 patients with 34 tumors. The mean time between the MRI examination and radical orchiectomy was 2.7 days. Patient selection is shown in Figure 1.

Magnetic Resonance Imaging Protocol

All MRI examinations were carried out using a 1.5-T MRI system (Magnetom Symphony, Siemens Medical Solutions, Erlangen, Germany) with a circular surface coil. Patients were examined in a supine position, with the testicles placed equidistant from the coil, utilizing a cloth placed beneath them, and with the penis resting on the lower abdominal wall. The MRI protocol consisted of the following sequences: unenhanced axial T1-weighted image (T1-WI), 3 planes (axial, coronal, and sagittal) T2-WI, axial DWI with *b*-values of 0, 400, and 800 s/mm^2, DCE images with 3-dimensional (3D) high temporal resolution. Gadopentetate dimeglumine (Gadovist, 0.2 mL per kilogram of body weight; Bayer Healthcare, Berlin, Germany) was introduced at a rate of 2 mL per second utilizing a power injector, succeeded by a subsequent infusion of 20 mL of normal saline. After IV contrast material injection, axial DCE images were obtained in 7 postcontrast phases with no interval between them. Also, coronal DCE images were obtained after injection. Table 1 details the technical parameters of the MRI sequences.

Magnetic Resonance Image Analysis

The MR images of 30 patients with 34 GCNIS-related TGCTs were transferred to a picture archiving communication system (PACS). The MRI data were interpreted in consensus by 2 radiologists (board-certified urogenital radiologist with >10 years of experience and a general radiologist with 8 years of experience, respectively). All radiologists were blinded to the histological data of the patients. Signal characteristics of the tumors on T2-WI were recorded, and the longest diameter (LD) was measured.

The DWI was evaluated with reference to axial T2-WI. Apparent diffusion coefficient (ADC) maps—were generated based on the high b-value DWI. For quantitative analysis, a circular region of interest (ROI) was defined as wide as possible within the tumor. The ROIs were meticulously drawn to omit artifacts and regions with hemorrhaging and/or necrosis, assisted by T1-WI, T2-WI, and DCE images. Tumor presence on ADC maps was defined as areas with low signal intensity (SI). Three measurements were made on the ADC maps, and the average was taken.

The enhancement patterns of tumors were evaluated on the maximum enhanced image and classified as heterogeneous or homogeneous. In addition, it was recorded whether there was a septal enhancement pattern within the tumor. The ROIs were placed in areas of tumors that showed maximum enhancement with care and with the aid of the corresponding T1- and T2-WI to exclude areas of hemorrhage and necrosis. Time SI (TSI) curves of the measured MRI signal for each ROI in arbitrary units plotted against time in seconds were compiled. The enhancement pattern was classified into 1 of 3 types according to the shape of the TSI curves: type I, a linear increase in enhancement over the entire dynamic period; type II, an initial upstroke followed by a plateau or mild-gradually increased; and type III, an initial upstroke followed by gradual washout. The TSI curves of all tumors were recorded. In addition, the measured SI from tumors $(S_i\ (i = 0, 1, .., 7))$ were normalized according to the formula $(S_i - S_o) / S_o$ with the help of precontrast SI (S_o). The following parameters first described by Tsili et al[8] were calculated using normalized measurements:

- Peak enhancement (PE) is described as the maximum *Si* of the tumor.
- Time to peak (TTP) is described as the time to reach the maximum *Si* of the tumor.
- Wash-in rate (WIR) is described as the maximum slope of tumor enhancement before TTP and calculated by the following formula; $WIR = max\ S_i\ (PE) - S_{i-1} / max\ t_i - t_{i-1}$
- Wash-out rate (WOR) is described as *maxSi (PE) – S7*, i.e., the difference between the maximum signal and the signal at the last time point.

MAIN POINTS

- Accurate characterization of testicular masses during the preoperative period is very important.
- Multiparametric magnetic resonance imaging can be used as a reliable preoperative method in the histological differentiation of germ cell neoplasia in situ-related testicular germ cell tumors.
- Reduced apparent diffusion coefficient values, low signal on T2-weighted imaging, and a septal enhancement pattern with high intensity in contrast to the tumor are imaging characteristics indicative of seminomas.
- Dynamic contrast-enhanced images have no proven role in the semin oma–non-seminomatous germ cell tumor distinction.

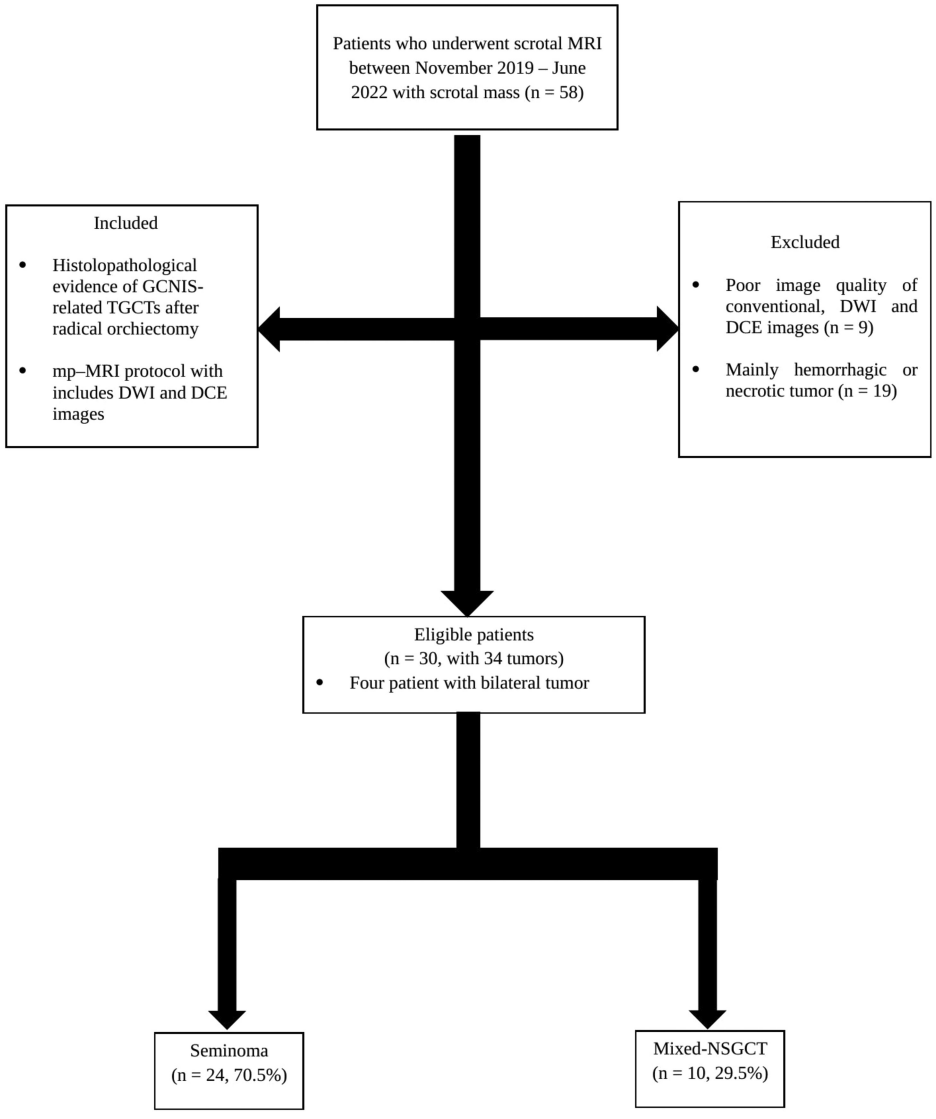

Figure 1. Flowchart of patient selection.
DCE, dynamic contrast-enhanced images; DWI, diffusion-weighted images; GCNIS, germ cell neoplasia in situ; MRI, magnetic resonance imaging; TGCT, testicular germ cell tumor.

Standard of Reference

A standard procedure of radical orchiectomy was performed for all tumors, with evaluation carried out by a pathologist possessing 15 years of expertise in the field of uropathology. The World Health Organization-2016 classification of TGCTs was used to classify the tumors. The pathologist was blinded to the mp-MRI findings during the evaluation.

Statistical Analysis

Statistical analyses were conducted using IBM Statistical Package for the Social Sciences Statistics software, version 25 (IBM SPSS Corp., Armonk, NY, USA). The assessment of data normality was carried out with the Kolmogorov–Smirnov test, and for normally distributed quantitative data, mean values were presented along with their corresponding SDs. Categorical variables were presented as numbers and percentages. The Mann–Whitney *U*-test was used to compare the mean values of ADC, PE, TTP, WIR, and WOR, and the LD between seminomas and mixed-NSGCTs. Receiver operating characteristic (ROC) curve analysis was performed to assess the diagnostic performance of parameters displaying distinct mean values between the 2 tumor groups. Statistical calculations were performed using 95% CIs. A P-value < .05 was considered statistically significant.

RESULTS

The study included 30 patients with 34 GCNIS-related TGCTs (mean ± SD, 35.2 ± 14.6 years; range, 26-89). In the study, 4 patients had bilateral tumors. Of the 34 GCNIS-related TGCTs, 24 (70.5%) were seminomas, and 10 (29.5%) were mixed-NSGCTs. Of the 10 mixed-NSGCTs, 4 (40%) were embryonal carcinoma and postpubertal teratoma, 2 (20%) were embryonal carcinoma, 2 (20%) were postpubertal yolk sac tumor, embryonal carcinoma, and postpubertal teratoma, and 2 (20%) were postpubertal yolk sac tumor and embryonal carcinoma.

The LDs were measured as 4.3 ± 2.4 cm and 3.6 ± 2.1 cm in seminoma and mixed-NSGCT cases, respectively. There was no significant difference between the 2 groups (P = .467). Twenty-four (20 seminomas and

Table 1. Technical Details of Multiparametric Magnetic Resonance Imaging Scanning Parameters

	T2-WI	T1-WI	DWI	DCE
Imaging planes	Axial, coronal, sagittal	Axial	Axial	Axial
Fat saturation	-	-	-	Fat-sat
Sequence	TSE	GRE	EPI	3D GRE
TE (ms)	100	15	110	4.1
TR (ms)	4000	500	4000	9
Flip angle (degrees)	90	90	90	35
NEX	2	1	12	1
FOV (cm)	24	24	24	22
Slice thickness	3	3	3	3
Matrix size	180 × 256	240 × 270	180 × 256	256 × 256
b value (s/mm^2)	-	-	0, 400, 800	-
Temporal resolution (s)	-	-	-	45
Number of acquisitions	-	-	-	7

DWI sequences included ADC map calculation.

ADC, apparent diffusion coefficient; DCE, dynamic contrast-enhanced images; DWI, diffusion-weighted images; EPI, Echo planar imaging; Fat-sat, fat saturated; FOV, field of view; GRE, Gradient recall echo; NEX, number of excitation; TE, time to echo; TR, time to repetition; TSE, Turbo spin echo; T1-WI, T1-weighted images; T2-WI, T2-weighted images.

4 mixed-NSGCTs) of the tumors were hypointense and 10 (4 seminomas and 6 mixed-NSGCTs) were isointense on T2-WI. Hypointense signal on T2-WI was statistically significant for seminomas compared to mixed-NSGCT ($P < .001$).

On DWI, all tumors showed restricted diffusion compared to normal testicular parenchyma (Figures 2, 3 and 4). The mean ADC values of the seminomas were statistically significantly lower than those of the mixed-NSGCTs (0.645 ± 0.11 and 0.879 ± 0.061, respectively, $P < .001$). Figure 5 clearly shows the difference between ADC value box plots for seminoma and mixed-NSGCTs. In the ROC curve analysis for ADC values, the area under the curve for the differentiation of seminoma and mixed-NSGCT was 0.983 (Figure 6). The optimal ADC cutoff point that simultaneously maximized sensitivity (91.6%), specificity (100%), and accuracy (94.1%) was 0.779 × 10^{-3} mm^2/s.

All tumors showed a type III TSI curve (Figures 2D, 3D, and 4D). In 14 (58.3%) of 24 seminomas, more intensely enhanced septa were observed compared to solid tumor areas (Figure 2C and 3C), whereas no enhanced septa was observed in any of the mixed-NSGCTs (Figure 4C) ($P = .002$). Table 2 presents the mean values of PE, TTP, WIR, and WOR for seminoma and mixed-NSGCT. There was no significant difference between the 2 groups for PE, TTP, WIR, and WOR ($P = .21$, .83, .31, and .16, respectively).

DISCUSSION

The results of our study showed that the measurement of ADC values, based on high *b*-value DWI, can largely distinguish between seminomas and mixed-NSGCTs since the cutoff value of 0.779 × 10^{-3} mm^2/s is used. Our results are similar to those previously reported in the literature.[9,10,23,24] In addition, in our study, DCE images showed the presence of septa with more intense enhancement compared to tumor tissue in most of the seminoma (58.3%), but this finding was not observed

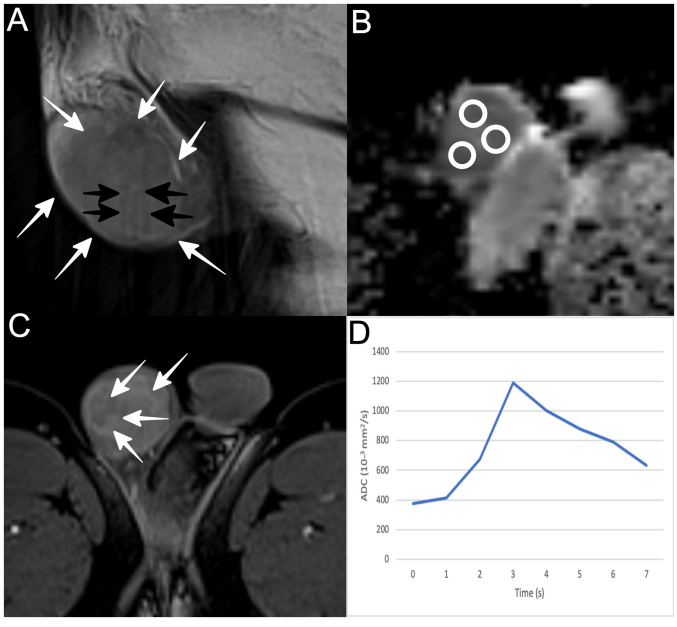

Figure 2. Right testicular seminoma in a 23-year-old man. (A) Sagittal T2-weighted image shows hypointense right testicular mass (white arrows). Tumor septa are also seen as hypointense bands (black arrows). (B) Axial ADC map (b = 800 s/mm^2) shows tumor's restricted diffusion. The mean ADC values of tumor (circular ROIs) were 0.49 × 10^{-3} mm^2/s. (C) Axial DCE image at early phase (180 seconds) shows heterogeneous tumor enhancement. Septal enhancement (arrows) more than the remaining tumoral tissue. (D) TSI curve shows early tumor enhancement, followed by gradual washout in the delayed phase (type III).
ADC, apparent diffusion coefficient; DCE, dynamic contrast-enhanced images; ROI, region of interest; TSI, time signal intensity.

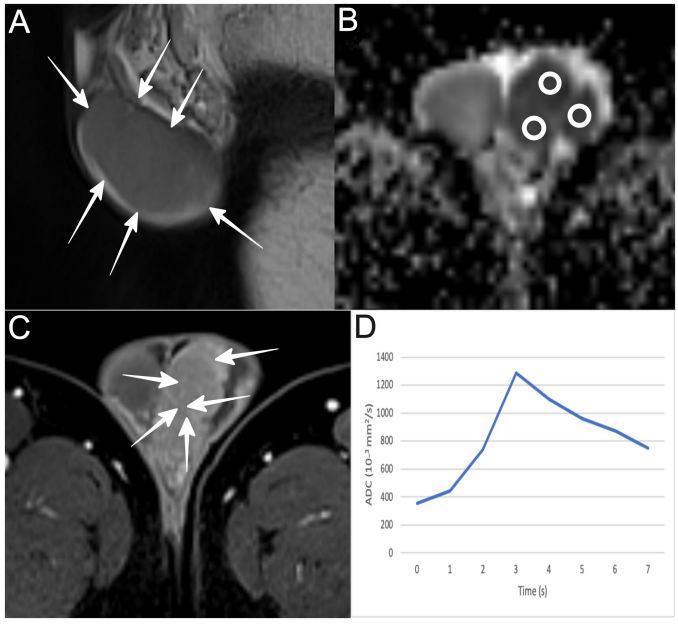

Figure 3. Left testicular seminoma in a 55-year-old man. (A) Sagittal T2-weighted image shows large hypointense left testicular mass (arrows), replacing the ipsilateral testis. (B) Axial ADC map (b = 800 s/mm^2) shows tumor's restricted diffusion. The mean ADC values of tumor (circular ROIs) were 0.53 × 10^{-3} mm^2/s. (C) Axial DCE image at early phase (180 seconds) shows heterogeneous tumor enhancement. Septal enhancement (arrows) more than the remaining tumoral tissue. (D) TSI curve is typical of malignancy (type III).
ADC, apparent diffusion coefficient; DCE, dynamic contrast-enhanced images; ROI, region of interest; TSI, time signal intensity.

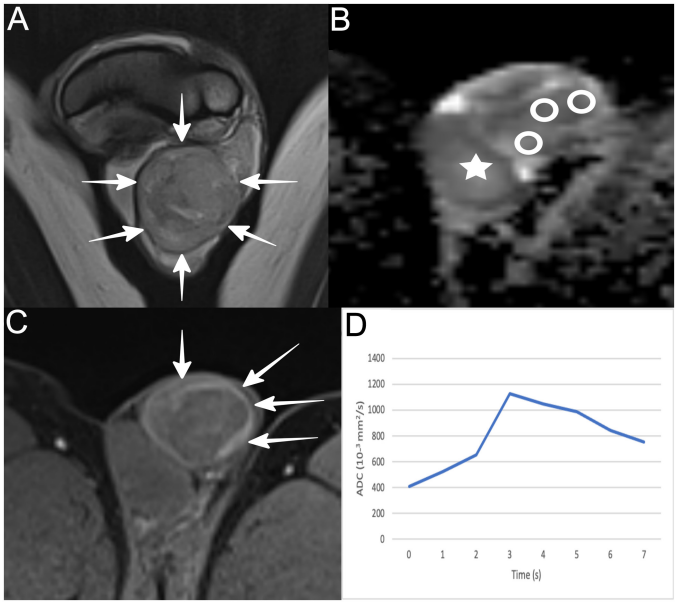

Figure 4. Left mixed-NSGCT (postpubertal type yolk sac, embryonal carcinoma, and postpubertal type teratoma) in a 31-year-old man. (A) Coronal T2-weighted image shows large heterogenous hypointense left testicular mass (arrows). (B) Axial ADC map (b = 800 s/mm^2) shows the tumor appears slightly hypointense compared to the contralateral testis (star) and has mild restricted diffusion. The mean ADC values (circular ROIs) of the tumor were 1.07×10^{-3} mm^2/s. (C) Axial DCE image in the early phase (180 seconds) shows nonhomogeneous circumferential tumor enhancement (arrows). Septal enhancement is absent. (D) TSI curve is typical of malignancy (type III).
ADC, apparent diffusion coefficient; DCE, dynamic contrast-enhanced images; NSGCT, non-seminomatous germ cell tumor; ROI, region of interest; TSI, time signal intensity.

in mixed-NSGCTs. This result is also similar to those previously reported by Tsili et al,[9] and the septal contrast enhancement pattern on DCE images suggests that it can be used to differentiate between seminoma and mixed-NSGCT. Also, we revealed that the majority of seminomas had a hypointense signal on T2-WI, and the presence of a hypointense signal on T2-WI was higher in seminomas compared to

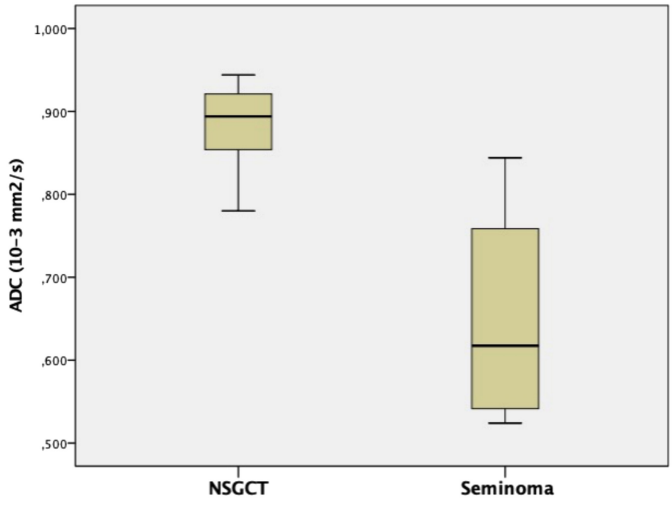

Figure 5. Box plots showing differences of ADC values between seminomas and mixed-NSGCT.
ADC, apparent diffusion coefficient; NSGCT, non-seminomatous germ cell tumor.

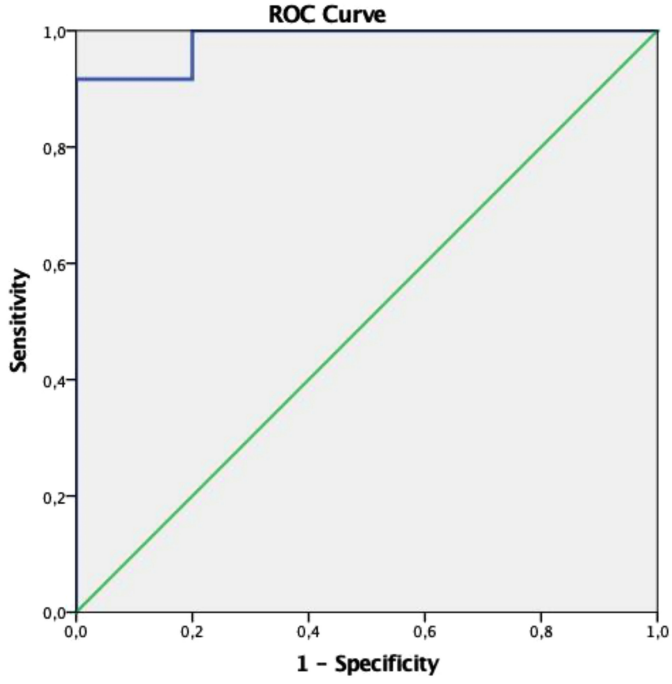

Figure 6. Receiver operating characteristic curve demonstrating the diagnostic performance of ADC values in differentiating seminomas from mixed-NSGCT.
ADC, apparent diffusion coefficient; NSGCT, non-seminomatous germ cell tumor; ROC, receiver operating characteristic curve.

mixed-NSGCTs ($P < .001$). This result was in parallel with studies that showed a close relationship between morphological imaging parameters and histological features of GCNIS-related TGCTs.[7,8]

As is known, radical orchiectomy is the preferred method for the treatment of GCNIS-related TGCTs and should be performed without delay. Nonetheless, in situations involving extensive disease and/or metastases that pose an immediate threat to life, emergency chemotherapy is warranted. Orchiectomy may be postponed until clinical stabilization has been attained.[1] It is very important to perform the histological characterization of GCNIS-related TGCTs with a non-invasive method in these cases.

More recently, morphological MRI sequences were found to be closely related to the histological features of GCNIS-related TGCTs.[7-10] Tsili et al[8] reported that 19 of 21 TGCTs were correctly classified preoperatively as seminoma or mixed-NSGCT in their study based on morphological MRI features. In our study, we showed that the T2-WI hypointense signal characteristic was identified with seminomas and was higher than mixed-NSGCTs ($P < .001$), similar to Tsili et al.[8] We think that this is due to the histological features of seminomas, which

Table 2. Mean Values of Relative Time Signal Intensity Parameters for Seminomas and Mixed-Non-Seminomatous Germ Cell Tumor

TSI Parameter	Seminoma (n = 24)	Mixed-NSGCT (n = 10)	*P*
PE	2.18 ± 0.87	3.08 ± 0.98	.21
TTP	4.18 ± 0.68	4.21 ± 0.75	.83
WIR	1.96 ± 0.64	2.02 ± 0.88	.31
WOR	0.18 ± 0.58	0.11 ± 0.51	.16

NSGCT, non-seminomatous germ cell tumor; PE, peak enhancement; TSI, time signal intensity; TTP, time to peak; WIR, wash-in rate; WOR, wash-out rate.

consist of a uniform population of large cells arranged in the lobules and cords. On the other hand, we think that mixed-NSGCTs have a more heterogeneous appearance compared to seminomas in morphological MRI parameters, due to the fact that they represent a large group consisting of different tumors and the higher frequency of necrosis.[5,7,9]

In our study, we performed ADC measurements based on high *b*-value DWI to distinguish between seminoma and mixed-NSGCT. Our results showed that ADC values were lower in seminomas compared to mixed-NSGCTs (0.645 ± 0.11 and 0.879 ± 0.061, respectively, $P < .001$). In addition, our results showed that seminoma-mixed-NSGCT discrimination can be made with high sensitivity, specificity, and accuracy when 0.779×10^{-3} mm^2/s is used as the optimal ADC cutoff value. Tsili et al[9] reported that the ADC values of seminomas were lower than those of mixed-NSGCT (0.59 ± 0.009 and 0.90 ± 0.33, respectively, $P < .001$) and showed that a seminoma-mixed-NSGCT distinction is possible with an optimal cutoff point of 0.68×10^{-3} mm^2/s for ADC values. Our results were similar to those previously reported in the literature. The diffusion restriction and low ADC values seen in seminomas are interpreted as secondary to the restriction of the mobility of water molecules due to histological features, such as the presence of large cells with abundant cytoplasm and large nuclei surrounded by fibrous trabeculae and accompanying lymphocyte infiltrates, plasma cells, eosinophils, and granulomatous reactions.[5,9,10]

While measuring ADC values in our study, we used a circular ROI by avoiding areas of necrosis and hemorrhage, and we took the average value by making 3 measurements from different areas of the tumor. There are limited studies in the literature regarding ROI-drawing techniques in the differentiation of GCNIS-related TGCTs. In the study of Tsili et al,[10] the use of multiple and circular ROIs and the calculation of the mean ADC value have been presented as the most useful methods in the histological characterization of GCNIS-related TGCT. It has been reported that the use of circular and multiple ROIs and obtaining average ADC values give more appropriate and accurate results in studies conducted for the differentiation of different testicular tumor groups for ADC measurement.[25,26] The results previously reported in the literature are similar to our study and show the accuracy of the ADC measurement results used in our study. We think that it is important to use multiple and circular ROIs when measuring ADC values to prevent possible false results due to the frequent occurrence of necrosis and hemorrhage, especially in mixed-NSGCTs, in the differentiation of GCNIS-related TGCTs.

In our study, a type III TSI curve was seen in DCE images in both seminoma and mixed-NSGCT cases. As is known, lesions with a type III TSI curve have a high PPV for the diagnosis of malignancy.[18,21,27-29] Previous studies by Tsili et al[9,22] reported that testicular tumors had a type III TSI curve. The type III TSI curve seen in tumors is thought to result from increased angiogenesis of the tumor, increased intratumoral arteriovenous shunts, and highly permeable vascular structures.[27-32] Further studies are needed to determine the utility of the type III TSI curve in distinguishing testicular tumors from benign processes. However, we believe that the TSI curves have no benefit for the histological differentiation of GCNIS-related TGCTs.

In our study, we also calculated 4 parameters from the TSI curves: PE, TTP, WIR, and WOR. We found that none of these parameters was statistically significant in the distinction between seminoma and mixed-NSGCT (P=.21, .83, .31, and .16, respectively). In previous studies, Tsili et al[9] reported that PE, TTP, WIR, and WOR parameters did not differ in the distinction between seminoma and mixed-NSGCT (P=.18, .63, .32, and .18, respectively), which is similar to our results. Tsili et al[21] reported in another study that only the relative maximum time (representing TTP) differed significantly between benign and malignant tumors ($P < .001$). As commonly recognized, tumor vascularity exhibits several characteristics linked to malignancies, such as spatial heterogeneity, disorganized structure, arteriovenous shunts, elevated vascular tortuosity and vasodilation, and the existence of inadequately developed fragile vessels featuring heightened permeability owing to the existence of large endothelial space cells.[9,27-29] We think that DCE images can be used in the differentiation of benign and malignant testicular masses because they are based on vascular patterns; however, they are not suitable for histological differentiation of GCNIS-related TGCTs because both seminomas and mixed-NSGCTs share the abovementioned features. However, we think that the septal contrast enhancement pattern, which we detected only in seminomas in our study, may help DCE images to distinguish between seminoma and mixed-NSGCT.

This study has some limitations. First, although it is the largest patient group in the literature to the best of our knowledge, it is a retrospective study conducted with a relatively small group of patients. In addition, mixed-NSGCTs represent a highly heterogeneous group, and the mp-MRI features of different histological subtypes may differ. Therefore, we think that multicenter studies with large patient populations are needed to perform histological characterization of GCNIS-related TGCTs in the preoperative period. Second, in our study, we did not use the whole tumor volume ROI for ADC measurements; we measured from 3 different points and averaged them. Although the whole tumor volume ROI is considered a reliable method, it is time-consuming and difficult to use in routine clinical practice. Third, MRI data were interpreted in consensus by the 2 radiologists; therefore, interobserver reliability was not assessed. Finally, we consider it possible that our findings could exhibit variations between and within scanners. This variability can be attributed to the significant differences in ADC measurements stemming from diverse factors, such as the types of coils, imagers, suppliers, and magnetic field strengths used for MRI. Despite these limitations, our study is the first to evaluate the histological differentiation of GCNIS-related TGCTs preoperatively using mp-MRI. We think that it will be a pioneer among the studies to be done on this subject.

Our study shows that mp-MRI including morphological images and ADC values, can be used as a reliable preoperative method in the histological differentiation of GCNIS-related TGCTs. The semiquantitative parameters obtained from DCE images have proven to be not specific enough to allow histological characterization of GCNIS-related TGCTs. Only the septal enhancement pattern on DCE images can be helpful in distinguishing between seminoma and mixed-NSGCT. Although histopathological examination remains the gold standard for the characterization of GCNIS-related TGCTs, larger prospective studies will help demonstrate the potential role of mp-MRI as a non-invasive method as an aid in the histological differentiation of these tumors.

Ethics Committee Approval: Ethics committee approval was received for this study from the ethics committee of Giresun University (Date: March 18, 2021, Number: KAEK-108).

Informed Consent: Due to its retrospective design, we waived the requirement for informed consent.

Peer-review: Externally peer-reviewed.

Author Contributions: Concept – S.A.; Design – S.A.; Supervision – U.O.; Materials – S.A., U.O.; Data Collection and/or Processing – S.A., U.E.; Analysis and/or Interpretation – İ.M.Ç; Literature Search – U.E; Writing Manuscript – S.A., U.E., İ.M.Ç.; Critical Review – U.O.

Declaration of Interests: The authors declare that they have no conflict of interest.

Funding: The authors declared that this study has received no financial support.

REFERENCES

1. Albers P, Albrecht W, Algaba F, et al. Guidelines on testicular cancer: 2015 update. *Eur Urol*. 2015;68(6):1054-1068. [CrossRef]
2. Yacoub JH, Oto A, Allen BC, et al. ACR appropriateness criteria staging of testicular malignancy. *J Am Coll Radiol*. 2016;13(10):1203-1209. [CrossRef]
3. American Cancer Society. Cancer facts & figures 2022. Available at: https://www.cancer.org/content/dam/cancer-org/research/cancer-facts-and-statistics/annual-cancer-facts-and-figures/2022/cancerfacts-and-figures-2022.pdf. Accessed 13 March 2022.
4. Moch H, Cubilla AL, Humphrey PA, Reuter VE, Ulbright TM. The 2016 WHO classification of tumours of the urinary system and male genital organs-part A: renal, penile, and testicular tumours. *Eur Urol*. 2016;70(1):93-105. [CrossRef]
5. Woodward PJ, Sohaey R, O'Donoghue MJ, Green DE. Tumors and tumor-like lesions of the testis: radiologic–pathologic correlation. *RadioGraphics*. 2002;22(1):189-216. [CrossRef]
6. Williamson SR, Delahunt B, Magi-Galluzzi C, et al. The World Health Organization 2016 classification of testicular germ cell tumours: a review and update from the International Society of Urological Pathology Testis Consultation Panel. *Histopathology*. 2017;70(3):335-346. [CrossRef]
7. Johnson JO, Mattrey RF, Phillipson J. Differentiation of seminomatous from nonseminomatous testicular tumors with MR imaging. *AJR*. 1990;154(3):539-543. [CrossRef]
8. Tsili AC, Tsampoulas C, Giannakopoulos X, et al. MRI in the histologic characterization of testicular neoplasms. *AJR*. 2007;189(6):W331-W337. [CrossRef]
9. Tsili AC, Sylakos A, Ntorkou A, et al. Apparent diffusion coefficient values and dynamic contrast enhancement patterns in differentiating seminomas from nonseminomatous testicular neoplasms. *Eur J Radiol*. 2015;84(7):1219-1226. [CrossRef]
10. Tsili AC, Ntorkou A, Astrakas L, et al. Diffusion-weighted magnetic resonance imaging in the characterization of testicular germ cell neoplasms: effect of ROI methods on apparent diffusion coefficient values and interobserver variability. *Eur J Radiol*. 2017;89:1-6. [CrossRef]
11. Oldenburg J, Berney DM, Bokemeyer C, et al. Testicular seminoma and non-seminoma: ESMO-EURACAN Clinical Practice Guideline for diagnosis, treatment and follow-up. *Ann Oncol*. 2022;33(4):362-375. [CrossRef]
12. Bhatt S, Jafri SZ, Wasserman N, Dogra VS. Imaging of nonneoplastic intratesticular masses. *Diagn Interv Radiol*. 2011;17(1):52-63. [CrossRef]
13. Dogra VS, Gottlieb RH, Oka M, Rubens DJ. Sonography of the scrotum. *Radiology*. 2003;227(1):18-36. [CrossRef]
14. Mathur M, Mills I, Spektor M. Magnetic resonance imaging of the scrotum: pictorial review with ultrasound correlation. *Abdom Radiol (NY)*. 2017;42(7):1929-1955. [CrossRef]
15. Tsili AC, Bertolotto M, Turgut AT, et al. MRI of the scrotum: recommendations of the ESUR Scrotal and Penile Imaging Working Group. *Eur Radiol*. 2018;28(1):31-43. [CrossRef]
16. Kim W, Rosen MA, Langer JE, Banner MP, Siegelman ES, Ramchandani P. Us MR imaging correlation in pathologic conditions of the scrotum. *RadioGraphics*. 2007;27(5):1239-1253. [CrossRef]
17. Mohrs OK, Thoms H, Egner T, et al. MRI of patients with suspected scrotal or testicular lesions: diagnostic value in daily practice. *AJR*. 2012;199(3):609-615. [CrossRef]
18. Tsili AC, Giannakis D, Sylakos A, Ntorkou A, Sofikitis N, Argyropoulou MI. MR imaging of scrotum. *Magn Reson Imaging Clin N Am*. 2014;22(2):217-238. [CrossRef]
19. Manganaro L, Vinci V, Pozza C, et al. A prospective study on contrast-enhanced magnetic resonance imaging of testicular lesions: distinctive features of Leydig cell tumours. *Eur Radiol*. 2015;25(12):3586-3595. [CrossRef]
20. Parenti GC, Feletti F, Carnevale A, Uccelli L, Giganti M. Imaging of the scrotum: beyond sonography. *Insights Imaging*. 2018;9(2):137-148. [CrossRef]
21. Tsili AC, Argyropoulou MI, Giannakis D, Sofikitis N, Tsampoulas K. MRI in the characterisation and local staging of testicular neoplasms. *AJR*. 2010;194(3):682-689. [CrossRef]
22. Tsili AC, Argyropoulou MI, Astrakas LG, et al. Dynamic contrast-enhanced subtraction MRI for characterizing intratesticular mass lesions. *AJR*. 2013;200(3):578-585. [CrossRef]
23. Algebally AM, Tantawy HI, Yousef RR, Szmigielski W, Darweesh A. Advantage of adding diffusion weighted imaging to routine MRI examinations in the diagnostics of scrotal lesions. *Pol J Radiol*. 2015;80:442-449. [CrossRef]
24. Tsili AC, Giannakis D, Sylakos A, et al. Apparent diffusion coefficient values of normal testis and variations with age. *Asian J Androl*. 2014;16(3):493-497. [CrossRef]
25. Inoue C, Fujii S, Kaneda S, et al. Apparent diffusion coefficient (ADC) measurement in endometrial carcinoma: effect of region of interest methods on ADC values. *J Magn Reson Imaging*. 2014;40(1):157-161. [CrossRef]
26. Mukuda N, Fujii S, Inoue C, et al. Apparent diffusion coefficient (ADC) measurement in ovarian tumor: effect of region-of-interest methods on ADC values and diagnostic ability. *J Magn Reson Imaging*. 2016;43(3):720-725. [CrossRef]
27. Sun MR, Ngo L, Genega EM, et al. Renal cell carcinoma: dynamic contrast-enhanced MR imaging for differentiation of tumor subtypes-correlation with pathologic findings. *Radiology*. 2009;250(3):793-802. [CrossRef]
28. Cornelis F, Tricaud E, Lasserre AS, et al. Routinely performed multiparametric magnetic resonance imaging helps to differentiate common subtypes of renal tumors. *Eur Radiol*. 2014;24(5):1068-1080. [CrossRef]
29. Ohno Y, Hatabu H, Takenaka D, et al. Dynamic MR imaging: value of differentiating subtypes of peripheral small adenocarcinoma of the lung. *Eur J Radiol*. 2004;52(2):144-150. [CrossRef]
30. Turkbey B, Kobayashi H, Ogawa M, Bernardo M, Choyke PL. Imaging of tumor angiogenesis: functional or targeted? *AJR*. 2009;193(2):304-313. [CrossRef]
31. Oto A, Yang C, Kayhan A, et al. Diffusion weighted and dynamic contrast-enhanced MRI of prostate cancer: correlation of quantitative MR parameters with Gleason score and tumor angiogenesis. *AJR*. 2011;197(6):1382-1390. [CrossRef]
32. Tuncbilek N, Kaplan M, Altaner S, et al. Value of dynamic contrast-enhanced MRI and correlation with tumor angiogenesis in bladder cancer. *AJR*. 2009;192(4):949-955. [CrossRef]